

Supporting Information

Discovery and isolation of the *trans*-isomers of two 1:2-type lanthanide-containing monolacunary Dawson-type tungstophosphates: $[\text{Ln}^{\text{III}}(\alpha_2\text{-P}_2\text{W}_{17}\text{O}_{61})_2]^{17-}$ (Ln = La, Ce)

Rong Wan, Pengtao Ma, Mengdan Han, Dongdi Zhang, Chao Zhang, Jingyang Niu* and Jingping Wang*

Henan Key Laboratory of Polyoxometalate Chemistry, Institute of Molecular and Crystal Engineering, College of Chemistry and Chemical Engineering, Henan University, Kaifeng, Henan 475004 P. R. China

Synthesis of compound 3 and 4

Table S1 Crystallographic data for 3 and 4

Fig. S1 The simulated (red) and experimental (black) powder XRD patterns of compounds 1–4.

Fig. S2 The structural comparison of the *trans*-isomers of (a) Keggin-type polyanions $[\text{Ln}^{\text{III}}(\text{PW}_{11}\text{O}_{39})_2]^{11-}$ (Ln = La, Ce) and Wells-Dawson-type polyanions $[\text{Ln}^{\text{III}}(\alpha_2\text{-P}_2\text{W}_{17}\text{O}_{61})_2]^{17-}$ (Ln = La, Ce).

Fig. S3 The solid-state ^{31}P NMR spectra of 1–4 at a spinning frequency of 12 kHz.

Fig.S4 The ^{31}P NMR spectra of (a) pure *trans*-La, (b) pure *cis*-La, (c) a physical mixture of *trans*-La and *cis*-La isomers in D_2O

Fig. S5 ESI-MS spectra of (a) *trans*-Ce and (b) *cis*-Ce dissolved in aqua solution in negative ion mode.

Fig. S6 Evolution of the ^{31}P NMR spectrum upon dissolution of pure *trans*-Ce with time in D_2O .

Fig. S7 Evolution of the ^{31}P NMR spectrum upon dissolution of pure *trans*-Ce as a function of pH value in $\text{H}_2\text{O}/\text{D}_2\text{O}$ (1:1).

Table S2 The ^{31}P NMR chemical shifts of species formed upon dissolution of pure *trans*-Ce in $\text{H}_2\text{O}/\text{D}_2\text{O}$ solution with different pH values.

Fig. S8 The ^{31}P NMR spectra of (a) pure *trans*-Ce, (b) pure *cis*-Ce, (c) a physical mixture of *trans*-Ce and *cis*-Ce isomers in D_2O and (d) adding *trans*-Ce into solution ($\text{D}_2\text{O}/\text{H}_2\text{O} = 1:1$) containing *cis*-Ce in alkaline solution (11.6).

Fig. S9 Evolution of the ^{31}P NMR spectrum of a physical mixture of isomers *trans*-Ce and *cis*-Ce in D_2O .

Fig. S10 ESI-MS spectrum of *trans*-Ce dissolved in aqua solution in negative ion mode: (a) pH = ca.11.5.

Fig. S11 IR Spectra of (a) the precipitate obtained from the solution above pH 12.8; (b) precursor $\text{Na}_{12}[\text{P}_2\text{W}_{15}\text{O}_{56}] \cdot 24\text{H}_2\text{O}$; (c) the precipitate obtained from the solution below pH 1.5; (d) precursor $\text{K}_6[\text{P}_2\text{W}_{18}\text{O}_{68}] \cdot 9\text{H}_2\text{O}$.

Fig. S12 The suggested dynamic transformation of 2 (*trans*-Ce) in $\text{H}_2\text{O}/\text{D}_2\text{O}$ (1:1) solution as the function of pH value.

TG analysis

Fig. S13 TG curves of **1** and **2**.

Cyclic voltammetry

Fig. S14 Cyclic voltammetric curves of **2** (*trans*-Ce), **4** (*cis*-Ce) and $K_{10}[\alpha_2\text{-P}_2\text{W}_{17}\text{O}_{61}]$.

Fig.S15 Evolution of cyclic voltammetric curves of **2** (*trans*-Ce) in aqua solution as a function of pH value.

Synthesis of compounds **3** and **4**

Synthesis of $((\text{CH}_3)_4\text{N})_{12}\text{Na}_3\text{H}_2[\text{La}(\text{P}_2\text{W}_{17}\text{O}_{61})_2]\cdot 26\text{H}_2\text{O}$ (**3**): the synthesis of **3** is similar to **1** but with pH was adjusted to 12.6 after the solid $\text{Na}_{12}[\text{P}_2\text{W}_{15}\text{O}_{56}]\cdot 24\text{H}_2\text{O}$ dissolved. Yield: 0.32 g (31.7% based on La). Elemental analysis: calcd for **3**: C, 5.83; H, 2.02; N, 1.70; Na, 0.70; La, 1.40; P, 1.25; W, 63.17%; Found: C, 5.96; H, 2.22; N, 1.69; Na, 0.71; La, 1.33; P, 1.19; W, 62.68%.

Synthesis of $((\text{CH}_3)_4\text{N})_{12}\text{Na}_3\text{H}_2[\text{Ce}(\text{P}_2\text{W}_{17}\text{O}_{61})_2]\cdot 26\text{H}_2\text{O}$ (**4**): The synthesis of **4** is similar to **3** but with $\text{CeCl}_3\cdot 6\text{H}_2\text{O}$ (0.025 g, 0.10 mmol) instead of $\text{LaCl}_3\cdot n\text{H}_2\text{O}$. Yield: 0.27 g (38.4% based on Ce). Elemental analysis (%): calcd for **4**: C, 5.83; H, 2.01; N, 1.70; Na, 0.70; Ce, 1.42; P, 1.25; W, 63.16%; Found: C, 5.89; H, 2.02; N, 1.61; Na, 0.74; Ce, 1.49; P, 1.20; W, 62.47%.

Table S1 Crystallographic data for **3** and **4**

	3	4
Empirical formula	$\text{Na}_3\text{C}_{48}\text{H}_{198}\text{N}_{12}\text{O}_{148}\text{P}_4\text{LaW}_{34}$	$\text{Na}_3\text{C}_{48}\text{H}_{198}\text{N}_{12}\text{O}_{148}\text{P}_4\text{CeW}_{34}$
Formula weight	9894.408	9895.618
Crystal system	monoclinic	monoclinic
Space group	$P2_1/c$	$P2_1/c$
a [Å]	29.122(11)	29.244(6)
b [Å]	25.143(7)	25.423(4)
c [Å]	33.754(2)	33.947(6)
β /°	114.544(6)	114.544(3)
Volume/Å ³	22482(2)	22895(7)
Z	4	4
$\rho_{\text{calc}}/\text{cm}^3$	2.884	2.757
μ/mm^{-1}	17.621	17.307
Data/parameters	39486/1228	40627/1104
R_{int}	0.0594	0.146
Goodness-of-fit on F^2	1.082	1.034
R_1, wR_2 [$I \geq 2\sigma(I)$]	0.0594, 0.145	0.0947, 0.2241
R_1, wR_2 [all data]	0.0801, 0.162	0.1800, 0.2711

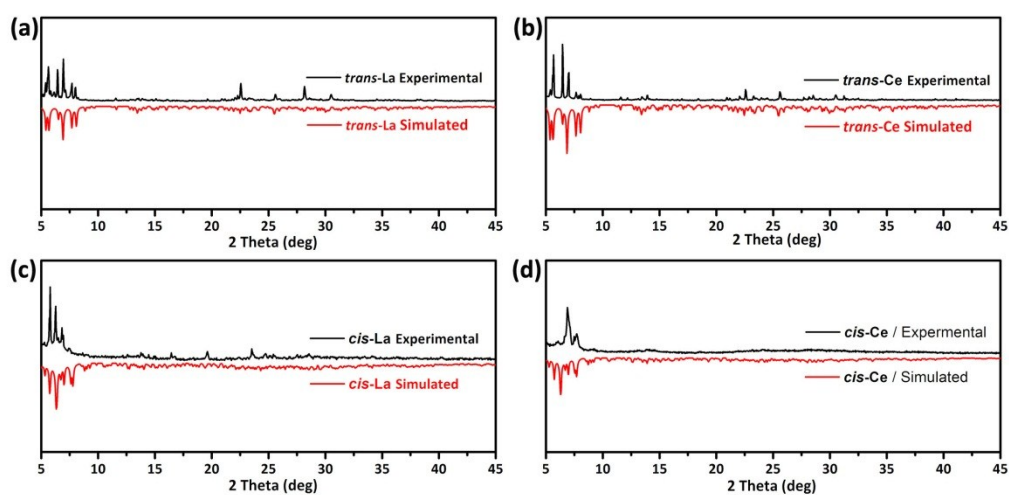


Fig. S1 The experimental and simulated powder XRD patterns of compounds (a) **1** (*trans*-La); (b) **2** (*trans*-Ce); (c) **3** (*cis*-La) and (d) **4** (*cis*-Ce).

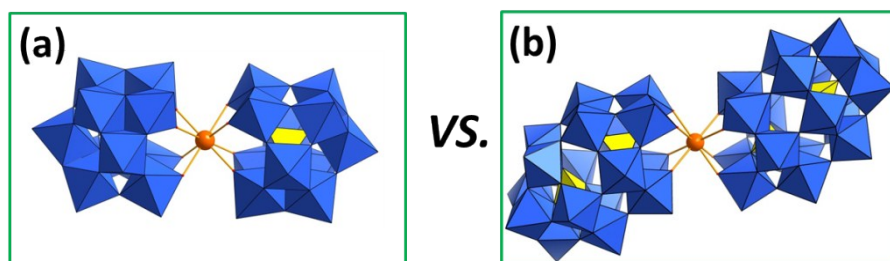


Fig. S2 The structural comparison of the *trans*-isomers of (a) Keggin-type polyanions $[\text{Ln}^{\text{III}}(\text{PW}_{11}\text{O}_{39})_2]^{11-}$ (Ln = La, Ce) and Wells-Dawson-type polyanions $[\text{Ln}^{\text{III}}(\alpha_2\text{-P}_2\text{W}_{17}\text{O}_{61})_2]^{17-}$ (Ln = La, Ce).

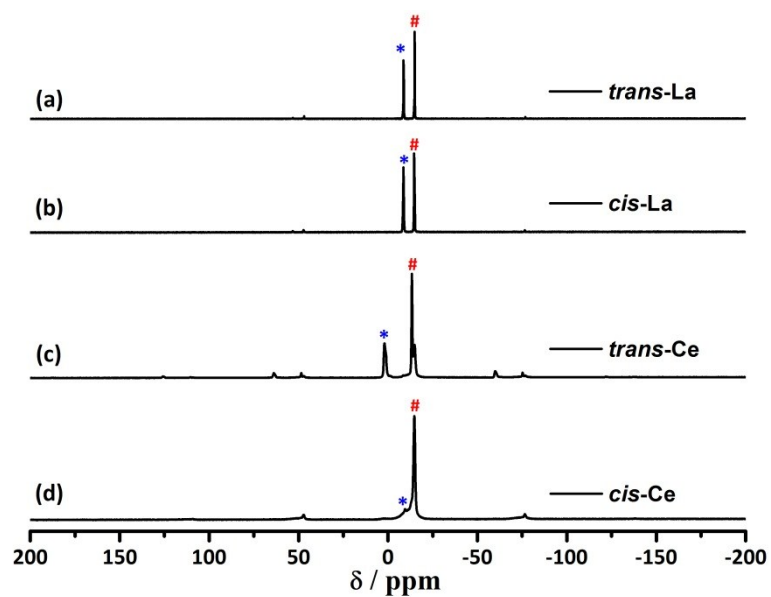


Fig. S3 The solid-state ^{31}P NMR spectra of **1–4** at a spinning frequency of 12 kHz. The center signals are marked with an asterisk (P1) and a pound (P2).

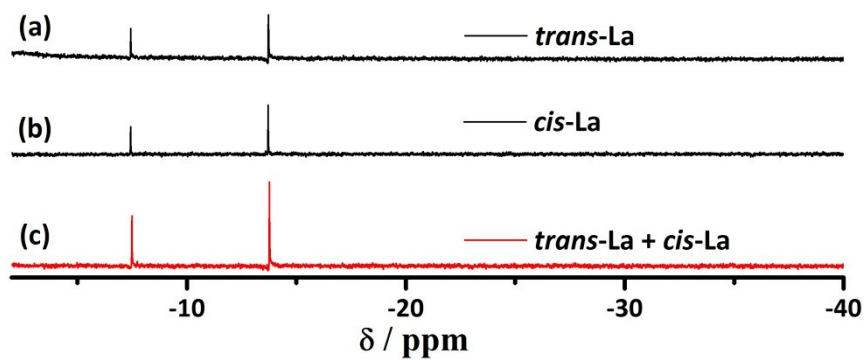


Fig.S4 The ^{31}P NMR spectra of (a) pure $trans\text{-La}$, (b) pure $cis\text{-La}$, (c) a physical mixture of $trans\text{-La}$ and $cis\text{-La}$ isomers in D_2O

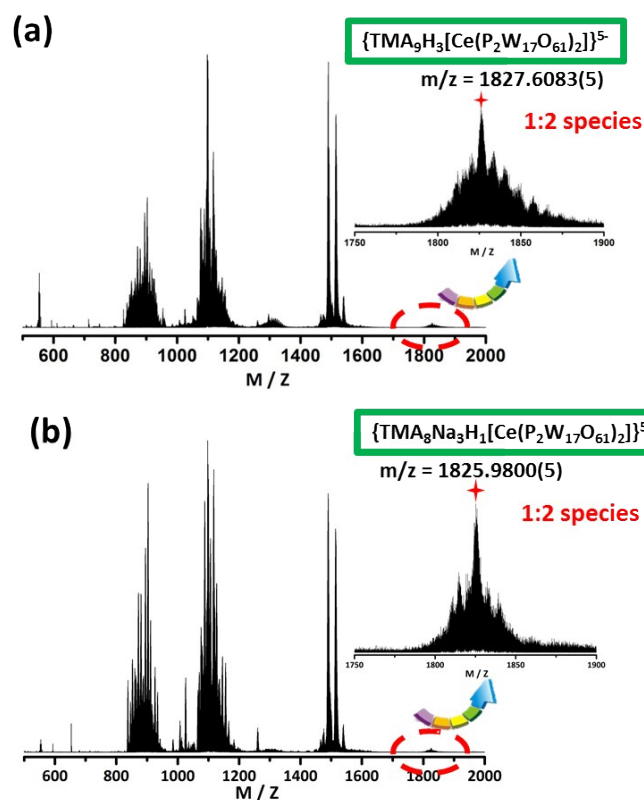


Fig. S5 ESI-MS spectra of (a) *trans*-Ce and (b) *cis*-Ce dissolved in aqua solution in negative ion mode. Concentration: 6×10^{-5} M. Inset: (a) Extension of the peak at m/z 1827.6083(5); (b) Extension of the peak at m/z 1825.9800(5).

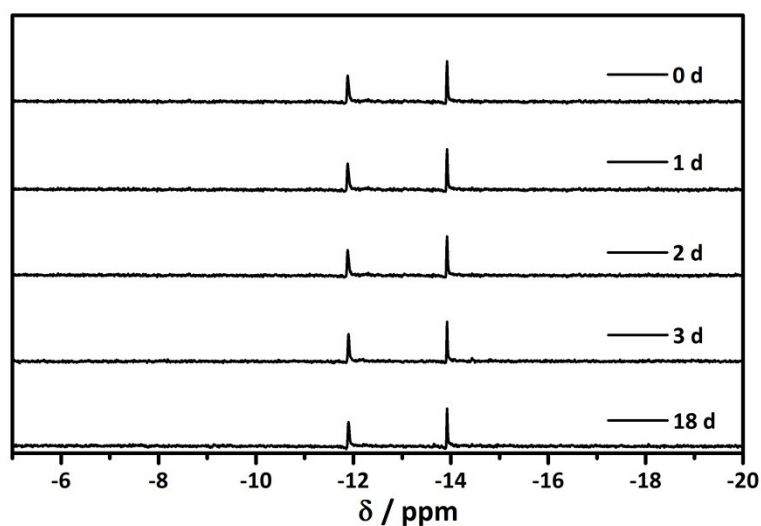


Fig. S6 Evolution of the ^{31}P NMR spectrum upon dissolution of pure *trans*-Ce with time in D_2O .

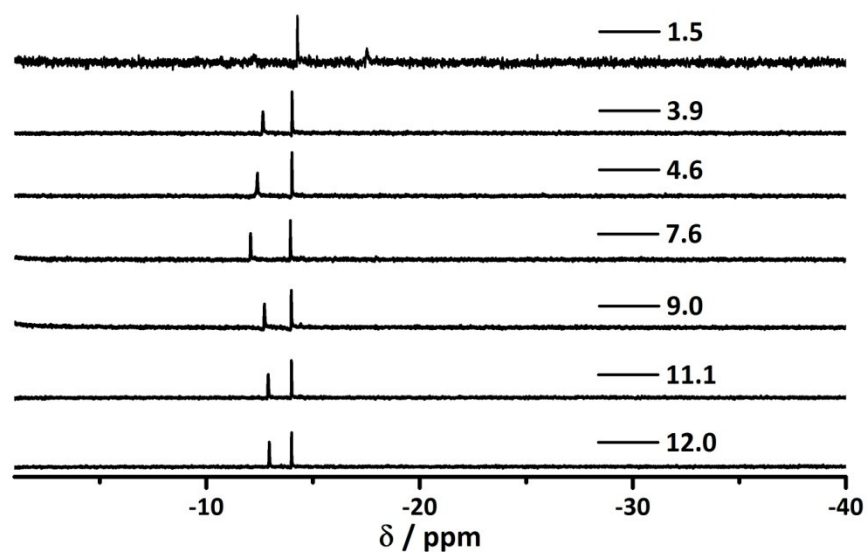


Fig. S7 Evolution of the ^{31}P NMR spectrum upon dissolution of pure *trans*-Ce as a function of pH value in $\text{H}_2\text{O}/\text{D}_2\text{O}$ (1:1).

Table S2 The ^{31}P NMR chemical shifts of species formed upon dissolution of pure *trans*-Ce in $\text{H}_2\text{O}/\text{D}_2\text{O}$ solution with different pH values.

pH	P1	P2	possible species
1.5	-14.27	-17.53	1:1-type LCMDP
3.9	-14.02	-12.66	<i>cis</i> -isomer
4.6	-14.01	-12.39	<i>cis</i> -isomer
7.6	-13.94	-12.07	<i>cis</i> -isomer
9.0	-13.98	-12.72	<i>cis</i> -isomer
10.1	-13.99	-12.84	<i>cis</i> -isomer
12.0	-14.00	-12.95	<i>cis</i> -isomer

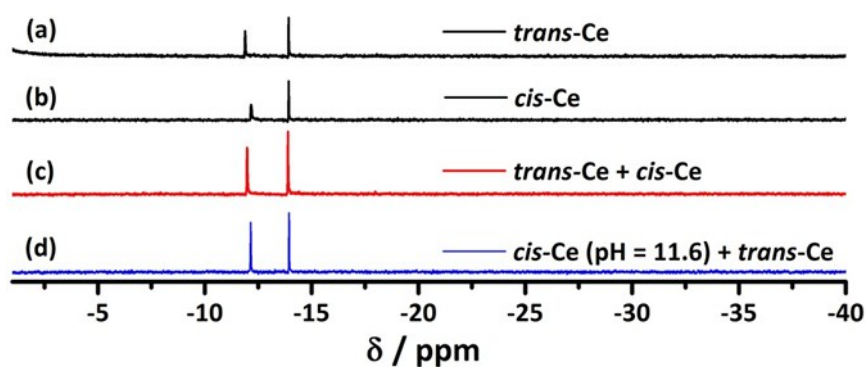


Fig. S8 ^{31}P NMR spectra of (a) pure *trans*-Ce, (b) pure *cis*-Ce, (c) a physical mixture of *trans*-Ce and *cis*-Ce isomers in D_2O and (d) adding *trans*-Ce into solution ($\text{D}_2\text{O}/\text{H}_2\text{O} = 1:1$) containing *cis*-Ce in alkaline solution (11.6).

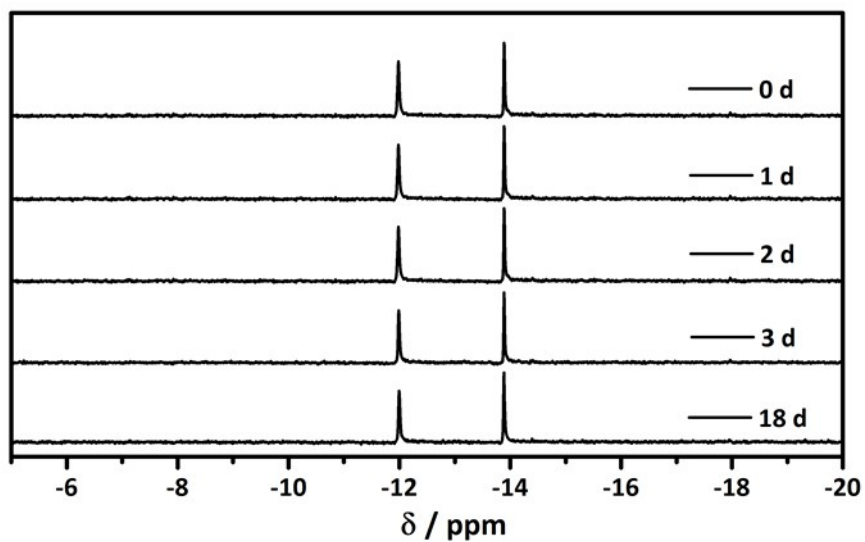


Fig.S9 Evolution of the ^{31}P NMR spectrum of a physical mixture of isomers *trans*-Ce and *cis*-Ce in D_2O .

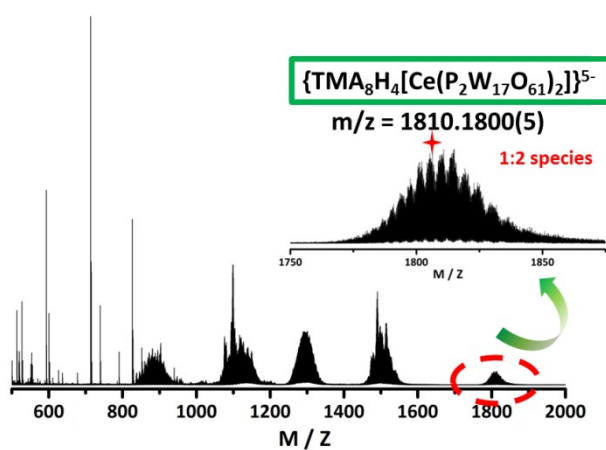


Fig. S10 ESI-MS spectrum of *trans*-Ce dissolved in aqua solution in negative ion mode (pH = ca.11.5). Concentration: 6×10^{-5} M. Inset: Extension of the peak at m/z 1810.1800(5).

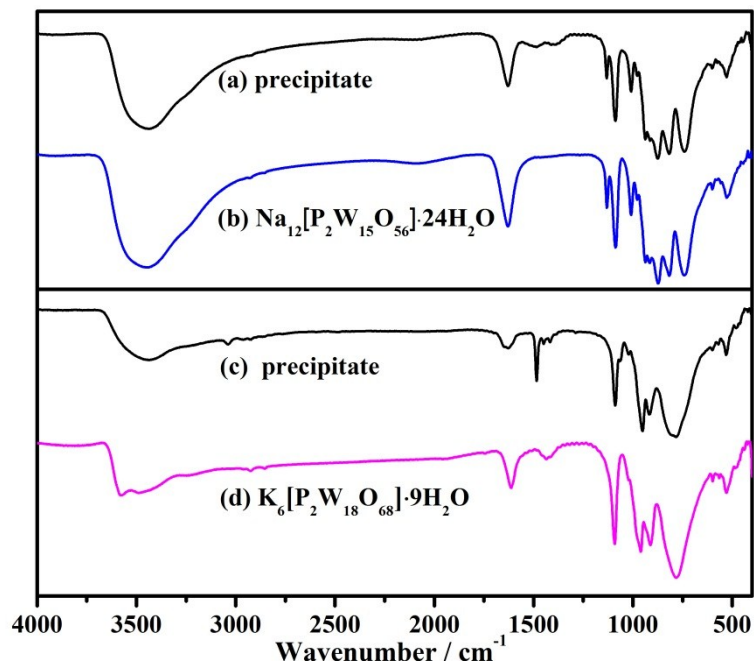


Fig. S11 IR Spectra of (a) the precipitate obtained from the solution above pH 12.8; (b) precursor Na₁₂[P₂W₁₅O₅₆]·24H₂O; (c) the precipitate obtained from the solution below pH 1.5; (d) precursor K₆[P₂W₁₈O₆₈]·9H₂O.

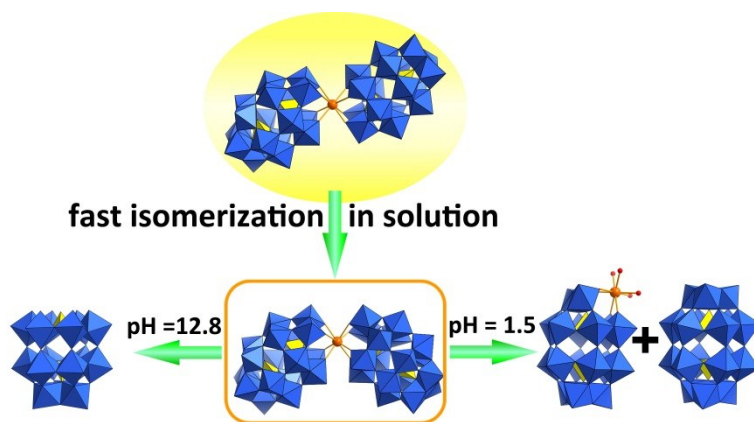


Fig. S12 The dynamic transformation of **2** (*trans*-Ce) in H₂O/D₂O (1:1) solution as the function of pH value.

TG analysis

The pyrolysis analysis of compound **1** and **2** were performed under N₂ ranging from the room temperature to 700 °C. As shown in Fig. S13, the TG curve of compound **1** and **2** both show two major weight loss stages in the regions of 25–275 and 225–565 °C. The observed first weight loss is 6.61 % for **1** (5.49% for **2**) from 25–275 °C, ascribed to the release of all the crystal water molecules and coordination water molecules (calculated 6.40 % for **1** and 5.43% for **2**). The second step of 225–565 °C gives a weight loss of 9.78 % for **1** (9.84% for **2**), which results from the release of TMA molecules (calculated 9.58 % for **1**/9.72 % for **2**).

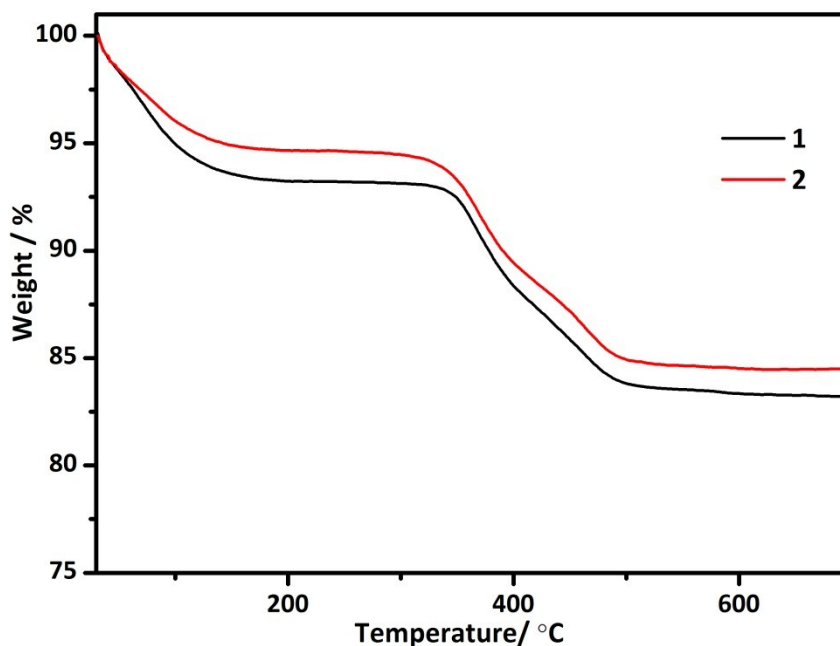


Fig. S13 TG curves of 1 and 2.

Cyclic voltammetry

The electrochemical behaviours of **2** (*trans*-Ce) and **4** (*cis*-Ce) were explored at room temperature in a standard three electrode cell connected to Shanghai Chenhua CGI660E B15375 electrochemical system. Cyclic voltammetric measurements of compound **2** and **4** and precursor $K_{10}[\alpha_2\text{-P}_2\text{W}_{17}\text{O}_{61}]$ (ca. $5 \times 10^{-4} \text{ mol}\cdot\text{L}^{-1}$) were carried out in the solution $\text{Na}_2\text{SO}_4 + \text{H}_2\text{SO}_4$ ($0.1 \text{ mol}\cdot\text{L}^{-1}$) at a scan rate of $5 \text{ mv}\cdot\text{s}^{-1}$. A freshly cleaned glassy carbon disk electrode (3 mm diameter) was used as a working electrode, a platinum wire served as the counter electrode and an Ag/AgCl electrode as the reference electrode. The electrochemical behaviors are investigated in the potential range of +1.0 to -1.4 V. As shown in the Fig. S14 and Table S3, the *trans*-Ce in solution (pH = 4.5) exhibits four pairs of redox waves of W(VI/V), which is very similar to the precursor $K_{10}[\alpha_2\text{-P}_2\text{W}_{17}\text{O}_{61}]$ apart from a little displacement. Besides, Similar results have also been obtained for other transition metal-substituted heteropolytungstates, for example, $[\alpha_2\text{-P}_2\text{W}_{17}\text{TiO}_{62}]^{8-}$, $[\alpha_2\text{-P}_2\text{W}_{17}\text{O}_{61}\text{Ir}^{\text{IV}}(\text{H}_2\text{O})]^{6-}$ and $[\alpha_2\text{-P}_2\text{W}_{17}\text{O}_{61}\text{Ru}^{\text{III}}(\text{H}_2\text{O})]^{7-}$.¹⁻² Compared with the cyclic voltammetric curve of precursor $K_{10}[\alpha_2\text{-P}_2\text{W}_{17}\text{O}_{61}]$, another one wave (V/V') was observed in *trans*-Ce and *cis*-Ce, which was attributed to redox wave Ce(IV/III).³ It is interesting that *trans*-Ce and *cis*-Ce have almost the same redox potentials. Moreover, the cyclic voltammograms of *trans*-Ce at different pH values (4.5–10.0) also exhibit very similar redox behaviors to *cis*-Ce in solution (Fig. S15). The main reason probably is that *trans*-Ce is apt to fast isomerize to *cis*-Ce, which also further confirmed by solid-state and solution ³¹P NMR spectra.

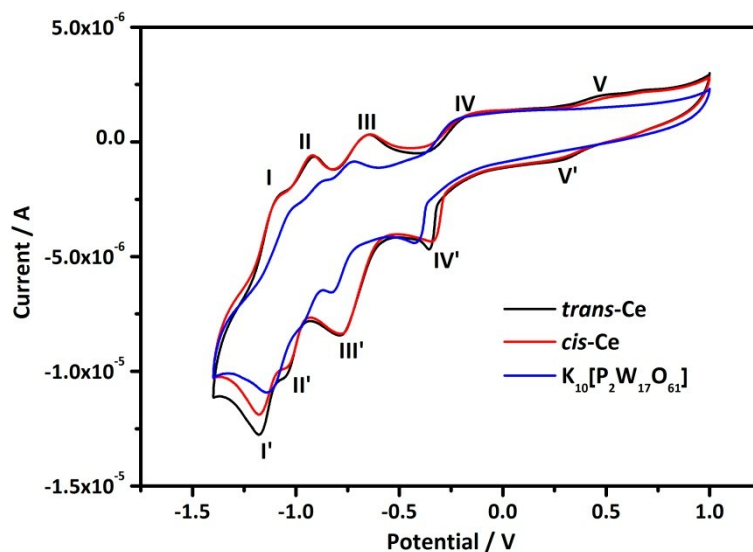


Fig. S14 Cyclic voltammetric curves of **2** (*trans*-Ce), **4** (*cis*-Ce) and $K_{10}[\alpha_2-P_2W_{17}O_{61}]$.

Table S3 Cyclic voltammetric data of **2** (*trans*-Ce), **4** (*cis*-Ce) and $K_{10}[\alpha_2-P_2W_{17}O_{61}]$ ^a

Compounds	<i>trans</i> -Ce			<i>cis</i> -Ce			$K_{10}[\alpha_2-P_2W_{17}O_{61}]$		
	E_{pa}/V	E_{pc}/V	$E_{1/2}/V$	E_{pa}/V	E_{pc}/V	$E_{1/2}/V$	E_{pa}/V	E_{pc}/V	$E_{1/2}/V$
I/I'	-1.09	-1.18	-1.14	-1.09	-1.18	-1.14	-1.02	-1.13	-1.08
II/II'	-0.93	-1.05	-0.99	-0.93	-1.04	-0.99	-0.89	-0.97	-0.93
III/III'	-0.65	-0.78	-0.72	-0.65	-0.78	-0.72	-0.73	-0.82	-0.47
IV/IV'	-0.16	-0.36	-0.26	-0.16	-0.34	-0.25	-0.21	-0.42	-0.32
V/V'	0.48	0.28	0.38	0.49	0.28	0.39	–	–	–

^a $E_{1/2} = (E_{pa} + E_{pc})/2$ (vs. the Ag/AgCl electrode)

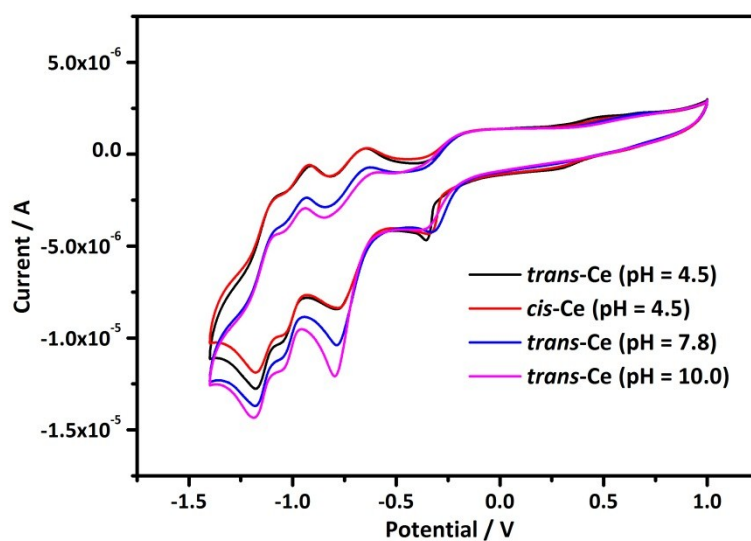


Fig.S15 Evolution of cyclic voltammetric curves of **2** (*trans*-Ce) in aqua solution with increasing pH.

References

- [1] J. Gong, Q.-J. Shan, D.-R. Wang, R.-N. Hua and L.-Y. Qu, *J. Electroanal. Chem.*, 1998, **455**, 39–44.
- [2] W. Sun, F. Yang, H. Liu, J. Kong, S. Jin, G. Xie and J. Deng, *J. Electroanal. Chem.*, 1998, **451**, 49–57.
- [3] M. Sadakane, M. H. Dickman, and M. T. Pope, *Inorg. Chem.* 2001, **40**, 2715-2719.